Top Curr Chem (2016) 368: 347–376
DOI: 10.1007/128_2015_638

Published online: 24 May 2015

Computational Molecular Electronic Spectroscopy with TD-DFT

Denis Jacquemin and Carlo Adamo

Abstract In this chapter we present applications of TD-DFT aiming at reproducing and rationalizing the optical signatures of molecules, and, more precisely, the absorption and fluorescence spectra of conjugated compounds belonging to both organic and inorganic families. We particularly focus on the computations going beyond the vertical approximation, i.e., on the calculation of 0–0 energies and vibronic spectra with TD-DFT, and on large applications performed for "real-life" structures (organic and inorganic dyes, optimization of charge-transfer structures, rationalization of excited-state proton transfer, etc.). We present a series of recent applications of TD-DFT methodology for these different aspects. The main conclusions of TD-DFT benchmarks aiming at pinpointing the most suited exchange-correlation functionals are also discussed.

Contents

D. Jacquemin (✉)
CEISAM, UMR CNRS 6230, Université de Nantes, 2, rue de la Houssinière, 44322 Nantes, France

Institut Universitaire de France, 103, blvd Saint-Michel, 75005 Paris, France
e-mail: Denis.Jacquemin@univ-nantes.fr

C. Adamo
IRCP UMR CNRS 8247, ENSCP-Chimie ParisTech, 11, rue Pierre et Marie Curie, 75005 Paris, France

Institut Universitaire de France, 103, blvd Saint-Michel, 75005 Paris, France

1 Introduction

By analyzing the continuously increasing number of quantum chemistry works relying on Time-Dependent Density Functional Theory (TD-DFT) [1–5], it appears that the vast majority of TD-DFT's applications are devoted to the modeling of the most widely available excited-state (ES) properties, namely optical spectra. One can roughly split these works into two major categories. In the first, which contains the majority of the TD-DFT investigations, the so-called vertical approximation is applied, i.e., a frozen ground-state (GS) geometry is considered and transition energies are determined without accounting for vibrational couplings [6]. This approach is computationally very efficient, allows one to characterize the nature of the relevant excited-states, and has been successfully used to design dyes or to understand environmental effects, albeit the vertical energies cannot be experimentally measured in most cases. However, more and more works of the second category, looking for well-grounded theory-measurement comparisons, have recently appeared. These studies, which imply higher computational efforts than their vertical counterparts, aimed at determining the 0–0 energies and/or vibrationally-resolved spectra [7–17]. Indeed, on the one hand, the 0–0 energies can be directly measured in the gas-phase for small molecules, or taken as the crossing point between absorption and emission curves (AFCP: absorption/fluorescence crossing point) in the experimental spectra of large solvates species [13], whereas, on the other hand, vibronic couplings give access to both band shapes and absolute intensities, which can also be directly correlated with measurements. The calculation of these properties implies the determination of the ES Hessian. Thanks to the development and implementation of analytic first and second derivatives [18–22], TD-DFT has indeed become an efficient approach to explore the potential energy surfaces (PES) of the ES in large compounds, the accuracy obtained being in most cases reasonable, at least close to the Franck–Condon point [23]. TD-DFT can therefore not only be used to probe the nature of the ES responsible for the absorption and fluorescence spectra but also provide many other properties, e.g., ES geometries and dipole moments, which are difficult (or costly) to measure

experimentally. Nevertheless, the application of TD-DFT to spectroscopic problems generally implies two major approximations: the use of the adiabatic approximation (i.e., only a frequency-independent exchange and correlation kernel is applied) and the selection of an adequate exchange-correlation functional (XCF). These two drawbacks limit the final accuracy of the results obtained and numerous works have been devoted to the appraisal of the most suited XCF [24], as well as to schemes going beyond linear-response TD-DFT [5, 25] in the framework of the simulation of optical spectra. Despite these limits, TD-DFT clearly remains the most applied theory for evaluating the spectral properties of "real-life" structures and this popularity can be ascribed to the simplicity and speed of use of this single-reference approach and also to the modeling of environmental effects which can be achieved with several theories [26, 27]. This general statement is particularly true for solvation effects for which a panel of refined models is now accessible [28–32].

In this chapter we summarize several recent advances in the TD-DFT spectroscopy field with a focus on recent works dealing with 0–0 energies, for which a protocol is detailed in Sect. 2. We next present the results of several benchmarks performed for these 0–0 energies (Sect. 3) before going through a series of examples obtained in the dye chemistry field (Sect. 4).

2 Protocol to Determine the 0–0 Energies

In this section we present a popular approach to compute the 0–0 energies with TD-DFT. This also allows us to define a series of different energies which are subsequently used, and to propose an easy-to-follow protocol to obtain all the relevant parameters which are represented in Fig. 1, in which R^{GS} and R^{ES} stand for the optimal geometries of the ground- and excited-states, respectively, whereas E^{GS} and E^{ES} are the total energies of these two states. Following [15], we first explain the more straightforward gas-phase situation before extending the protocol to the condensed phase.

2.1 Gas Phase

In the gas phase, the vertical absorption can simply be defined as the difference between the ES and GS energies at the optimal ground-state geometry,

$$E^{\text{vert}-\text{a}} = E^{\text{ES}}\left(R^{\text{GS}}\right) - E^{\text{GS}}\left(R^{\text{GS}}\right), \tag{1}$$

whereas the vertical fluorescence is the corresponding data estimated at the optimal geometry of the relevant excited-state,

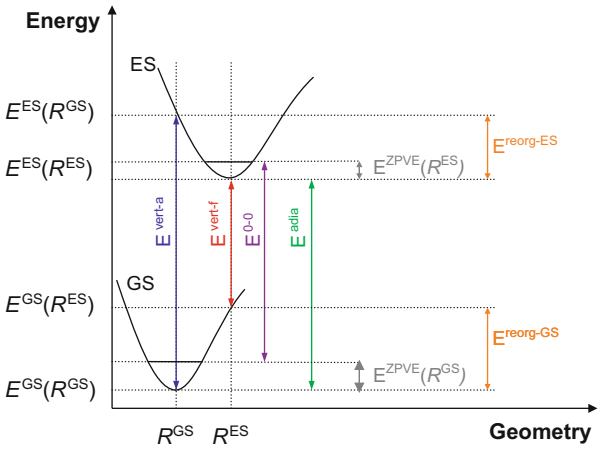

Fig. 1 Simplified energy diagram representing only two singlet states without intersections and describing key theoretical parameters. Reproduced with permissions from Jacquemin et al. [15]. Copyright 2012, American Chemical Society

$$E^{\text{vert}-\text{f}} = E^{\text{ES}}\left(R^{\text{ES}}\right) - E^{\text{GS}}\left(R^{\text{ES}}\right). \tag{2}$$

We note that the second quantity implies a force minimization process performed at the ES to define R^{ES}, and can be obtained efficiently with a wide panel of quantum chemistry codes which include analytical TD-DFT gradients (e.g., Gaussian, Turbomole, Q-Chem, and NWChem to cite a few) [18–20]. The adiabatic energy can be obtained as a simple by-product of the two previous equations,

$$E^{\text{adia}} = E^{\text{ES}}\left(R^{\text{ES}}\right) - E^{\text{GS}}\left(R^{\text{GS}}\right), \tag{3}$$

or, alternatively by combining vertical transition energies with the geometrical reorganization energies,

$$E^{\text{adia}} = \frac{1}{2}\left[E^{\text{vert}-\text{f}} + E^{\text{vert}-\text{a}}\right] + \frac{1}{2}\left[E^{\text{reorg}-\text{GS}} - E^{\text{reorg}-\text{ES}}\right]. \tag{4}$$

In this latter equation the first term tends to be dominant, and, in a first crude approximation the second term can be neglected. Indeed, the second term is the difference of reorganization energies between the two considered states, which is significant only when there is a strong difference between R^{GS} and R^{ES}. Next, one needs to determine the difference of zero-point vibrational energy (ZPVE) between the ES and GS,

$$\Delta E^{\text{ZPVE}} = E^{\text{ZPVE}}\left(R^{\text{ES}}\right) - E^{\text{ZPVE}}\left(R^{\text{GS}}\right), \tag{5}$$

a computationally demanding term, as second derivatives (Hessian) of the ES PES need to be computed, either analytically [21, 22] or numerically. For small molecules, at least, comparisons with the results obtained using wavefunction

approaches, demonstrated that TD-DFT generally provides accurate ΔE^{ZPVE} [17]. To reach the 0–0 energies, one adds the two previous terms:

$$E^{0-0} = E^{\mathrm{adia}} + \Delta E^{\mathrm{ZPVE}}. \tag{6}$$

We note that ΔE^{ZPVE} is almost systematically negative, as the PES of the ES tends to be flatter than its GS counterpart and, consequently, E^{0-0} is generally smaller than E^{adia}. As stated above, E^{0-0} can be directly compared to the absorption-fluorescence crossing point for solvated molecules, and it subsequently offers a much more solid basis for theory–experiment comparisons than $E^{\mathrm{vert-a}}$, which often has no straightforward experimental counterpart.

2.2 Condensed Phase

When considering an environment surrounding the molecule of interest (the compound undergoing the electronic transition), it is crucial to determine how the medium reacts to the change of electronic state of the photo-active compound. Irrespective of the nature of the environment, one distinguishes the equilibrium (eq) and non-equilibrium (neq) regimes [26]. In the former, a full (electrons and nuclei) medium relaxation takes place, and such a regime is adapted to determine "slow properties", e.g., both R^{ES} and $E^{\mathrm{ZPVE}}(R^{\mathrm{ES}})$. Essentially, it implies that the dye-environment interactions can be accounted for in a similar way as in the GS. In the latter neq limit, only the electronic cloud of the medium can adapt to the new electronic configuration of the chromophore, and this scheme is useful to model rapid phenomena, typically transition energies. Indeed, the vertical transition energies now read

$$E^{\mathrm{vert-a}}(\mathrm{neq}) = E^{\mathrm{ES}}\left(R^{\mathrm{GS}}, \mathrm{neq}\right) - E^{\mathrm{GS}}\left(R^{\mathrm{GS}}, \mathrm{eq}\right), \tag{7}$$

for absorption, and

$$E^{\mathrm{vert-f}}(\mathrm{neq}) = E^{\mathrm{ES}}\left(R^{\mathrm{ES}}, \mathrm{eq}\right) - E^{\mathrm{GS}}\left(R^{\mathrm{ES}}, \mathrm{neq}\right), \tag{8}$$

for emission. For the former phenomenon, one starts from an eq GS and goes to a neq ES, whereas for the latter phenomenon, the ES is in equilibrium whereas the GS is in non-equilibrium, and a proper modeling of the latter process requires quite advanced computational approaches [30–32]. Differences between eq and neq vertical transition energies can be significant in polar solvents [26]. By definition, both the adiabatic and 0–0 energies are equilibrium properties as they correspond to a transition between two states at their respective minima:

$$E^{0-0}(\text{eq}) = E^{\text{adia}}(\text{eq}) + \Delta E^{\text{ZPVE}}(\text{eq}). \tag{9}$$

However, this raises a difficulty, because the experimental absorption-fluorescence crossing point corresponds to the intersection of two curves in the experimental spectra, each being associated with a neq phenomenon. This cannot be properly modeled by the use of (9). To resolve this inconsistency, it has been proposed to correct the $E^{0-0}(\text{eq})$ in the following way [33]:

$$E^{\text{AFCP}}(\text{neq}) = E^{0-0}(\text{eq}) + \frac{1}{2}\left[\Delta E^{\text{vert}-\text{a}} + \Delta E^{\text{vert}-\text{f}}\right], \tag{10}$$

where the correcting terms are

$$\Delta E^{\text{vert}-\text{a}} = E^{\text{vert}-\text{a}}(\text{neq}) - E^{\text{vert}-\text{a}}(\text{eq}), \tag{11}$$

$$\Delta E^{\text{vert}-\text{f}} = E^{\text{vert}-\text{f}}(\text{neq}) - E^{\text{vert}-\text{f}}(\text{eq}). \tag{12}$$

The rationale for this correction can be obtained by examining (4). Indeed, in (10), the only approximations are the neglect of the difference between non-equilibrium and equilibrium environmental effects on the difference between the reorganization energies of the two states, a very small contribution, and the consideration of equilibrium limit during the computation of ΔE^{ZPVE}, but the eq–neq variations for this average term are generally trifling.

2.3 *Further Comments*

2.3.1 Calculations with the Polarizable Continuum Model

The most popular approach for modeling solvent effects is the Polarizable Continuum Model (PCM) which treats the environment as a structureless material presenting the macroscopic properties of the actual solvent. The solute is embedded in a cavity inside this solvent, and charges located on the surface of this cavity are determined self-consistently to account for the electrostatic interactions between the solute and the solvent [26]. We briefly describe here the different variations of the PCM model which have been developed for ES. In the (simplest) linear response (LR) model [28, 29], the GS-to-ES transition densities are used to determine the variations of the charges localized on the cavity when the solute changes its electronic configuration. In the corrected linear response (cLR) [30], the one-particle TD-DFT density matrix (the actual density of the ES within the selected approximation) is used in a perturbative approach, to evaluate the changes of the charges of the cavity when the solute changes electronic state [30]. The use of the one-particle TD-DFT density, rather than the transition density, advantageously allows one to account for orbital relaxation, and this density is also used in the two

self-consistent approaches, namely the state specific (SS) [31] and the vertical excitation model (VEM) [32] approaches. One of the principal differences between the two approaches is that the former implies a modification of the GS reference during the self-consistent process, whereas the latter does not. When the change of polarity of the chromophore between the GS and ES is large, e.g., for charge-transfer (CT) transitions, going beyond the LR-PCM approximation is recommended, though the most adequate model in that case remains a matter of debate [34, 35].

We underline that, although all these approaches can be used to determine E^{ES} analytically, analytic gradients (and hence efficient access to R^{ES}) are only available with the LR approach [20]. Subsequently, a popular approach is to determine $E^{\mathrm{vert-a}}$, $E^{\mathrm{vert-f}}$, and E^{adia} with one of the three refined PCM approaches (cLR, SS, and VEM) on geometries computed within the LR-PCM model. Likewise, ΔE^{ZPVE} is often calculated at the LR-PCM level, so that the results of (10) are generally obtained with mixed environmental models, the energy (geometry and vibrations) being obtained with a refined (simpler) PCM level of theory [33].

2.3.2 0–0 Energies with Mixed DFT/Wavefunction Approaches

Besides TD-DFT, there is a wide panel of alternative and (very) accurate ab initio methods with, on the one hand, multi-reference approaches, e.g., Complete Active Space second-order Perturbation Theory (CAS-PT2) [36] and Multi-Reference Configuration Interaction (MR-CI) [37], and, on the other hand, single-reference (highly-)correlated schemes, e.g., Equation-of-Motion Coupled Cluster (EOM-CC) [38–41], Symmetry Adapted Cluster CI (SAC-CI) [42], Algebraic Diagrammatic Construction (ADC) [43], and Configuration Interaction singles with a perturbative correction for double excitations [CIS(D)] [44, 45]. Despite the rapid developments of these approaches and the implementations of efficient protocols (e.g., the resolution of identity scheme), their less favorable scalings with system size than TD-DFT generally limit their applications to vertical calculations but for rather small molecules. Therefore, it has been proposed to combine TD-DFT's ES geometries and vibrations to $E^{\mathrm{vert-a}}$ and $E^{\mathrm{vert-f}}$ obtained with these more advanced approaches. In the protocol proposed by Goerigk and Grimme [13], the experimental 0–0 energies are first transformed into "experimental" vertical energies by applying successive corrections for solvation, vibration, and geometrical reorganization effects determined with TD-DFT. Alternatively, one can determine AFCP energies through (10) and next correct them through wavefunction (Ψ) vertical calculations performed on the DFT GS and TD-DFT ES geometries [46, 47]. For approaches that can only be used for gas-phase vertical transition energies, the corrected AFCP energy simply becomes

$$E_{\mathrm{BE}}^{\mathrm{AFCP}}(\mathrm{neq}) = E_{\mathrm{TD-DFT}}^{\mathrm{AFCP}}(\mathrm{neq}) + \left[E_{\Psi}^{\mathrm{adia}}(\mathrm{gas}) - E_{\mathrm{TD-DFT}}^{\mathrm{adia}}(\mathrm{gas})\right], \qquad (13)$$

where BE stands for best estimates. Compared to (10), (13) only requires, for the TD-DFT part, two additional vertical gas-phase calculations (one for each optimal geometry) and the time-limiting step generally remains the wavefunction computation. The accuracy of the results obtained with (13) of course depends not only on the quality of the wavefunction model but also partly on the "starting" accuracy obtained with TD-DFT. When TD-DFT strongly underestimates the transition energies, using (13) could be less efficient.

2.3.3 Band Shapes

Once the GS and ES vibrational signatures have been determined, for instance in the course of computing the ΔE^{ZPVE} contribution to E^{0-0}, it is possible to obtain vibronic couplings and hence to estimate absorption and emission band shapes. This requires the calculation of the coupling factors between the different vibrational states of the GS and the ES, a task often achieved by the Franck–Condon (for strongly dipole allowed transitions) and/or Herzberg–Teller (for forbidden or weakly allowed transitions) approaches [7, 9, 12, 48–51]. Such schemes are now implemented in several codes, and can also be used to gain access to absolute intensities, i.e., the molar absorptivity (generally noted ε in the well-known Beer–Lambert's law). This offers additional direct comparisons with experimental data.

2.3.4 Choice of an Exchange-Correlation Functional

Though this topic is discussed in more detail in Sect. 3, is it probably worth giving some general comments regarding the selection of an appropriate XCF. First, one can select a hybrid functional, incorporating a fraction of the so-called *exact* exchange: they generally yield much more accurate results than the typical LDA or GGA approaches which tend to provide much too low transition energies in most compounds. If valence ES are investigated, one should distinguish the localized ES, typically resulting for $n \rightarrow \pi^\star$ and $\pi \rightarrow \pi^\star$ transitions, for which standard global hybrids such as B3LYP [52] or PBE0 [53] are well suited from charge-transfer excited-states, for which the selection of range-separated hybrids which present an amount of *exact* exchange increasing with the interelectronic distance, e.g., CAM-B3LYP [54] of ωB97X-D [55], generally provide more accurate transition energies. Eventually, range-separated hybrids are also often a better choice for Rydberg ES [56].

2.3.5 Choice of an Atomic Basis Set

Similar to DFT, TD-DFT is relatively less sensitive to the size of the atomic basis set than the corresponding highly-correlated wavefunction theories, though exceptions have been reported [57]. Irrespective of the agreement with experimental data, reaching ES data which are converged with respect to the extension of the basis set generally requires the selection of larger atomic basis sets than for GS properties. For electronic transitions to low-lying excited-states in conjugated molecules, a double-ζ (or, better, triple-ζ) polarized atomic basis set augmented with diffuse orbitals appears to be a judicious choice. In other words, 6-31+G(d) or *aug*-cc-pVDZ could be advised as reasonable compromises between computational cost and accuracy for both $E^{\text{vert}-\text{a}}$ and $E^{\text{vert}-\text{f}}$. Of course, for Rydberg ES, a much larger basis set may be necessary, e.g., *aug*-cc-pVTZ. When optimizing the geometry of a given ES, one should also be cautious as the PES are often quite flat and diffusionless basis sets could yield rather poor results but in strongly constrained fluorophores. The interested reader can find elsewhere longer discussions regarding basis set effects for both small [58] and large [15] molecules in the context of TD-DFT spectroscopic investigations.

3 Benchmarks

In this section we present the results obtained in several benchmarks aiming to pinpoint the most adequate XCF. Both 0–0 energies and band topologies, obtained through the calculation of vibronic couplings, are discussed. A general statement, at least applicable to low-lying ES of organic molecules, is that pure XCF which do not include exact exchange (e.g., BLYP [59, 60] or PBE [61]) tend to provide much poorer results than hybrid XCF. In global hybrid functionals (e.g., B3LYP [52], PBE0 [53, 62], and M06-2X [63, 64]) the main parameter affecting the computed E^{AFCP} is the mixing between the exact and DFT exchange, whereas in range-separated hybrids (e.g., CAM-B3LYP [54] and ωB97X-D [55]), the attenuation parameter which defines the rate at which one goes from DFT to exact exchange is the key parameter. We redirect the interested readers to [24] for a longer and more general review of existing TD-DFT benchmarks.

3.1 AFCP Energies

In this section we focus on investigations treating the E^{AFCP} of large molecules [7, 13, 15, 65], though there are several works dealing with small gas-phase compounds for which the 0–0 band can be accurately measured [17, 19, 66–69]. First, as ΔE^{ZPVE} is the most computationally expensive term, let us discuss its magnitude

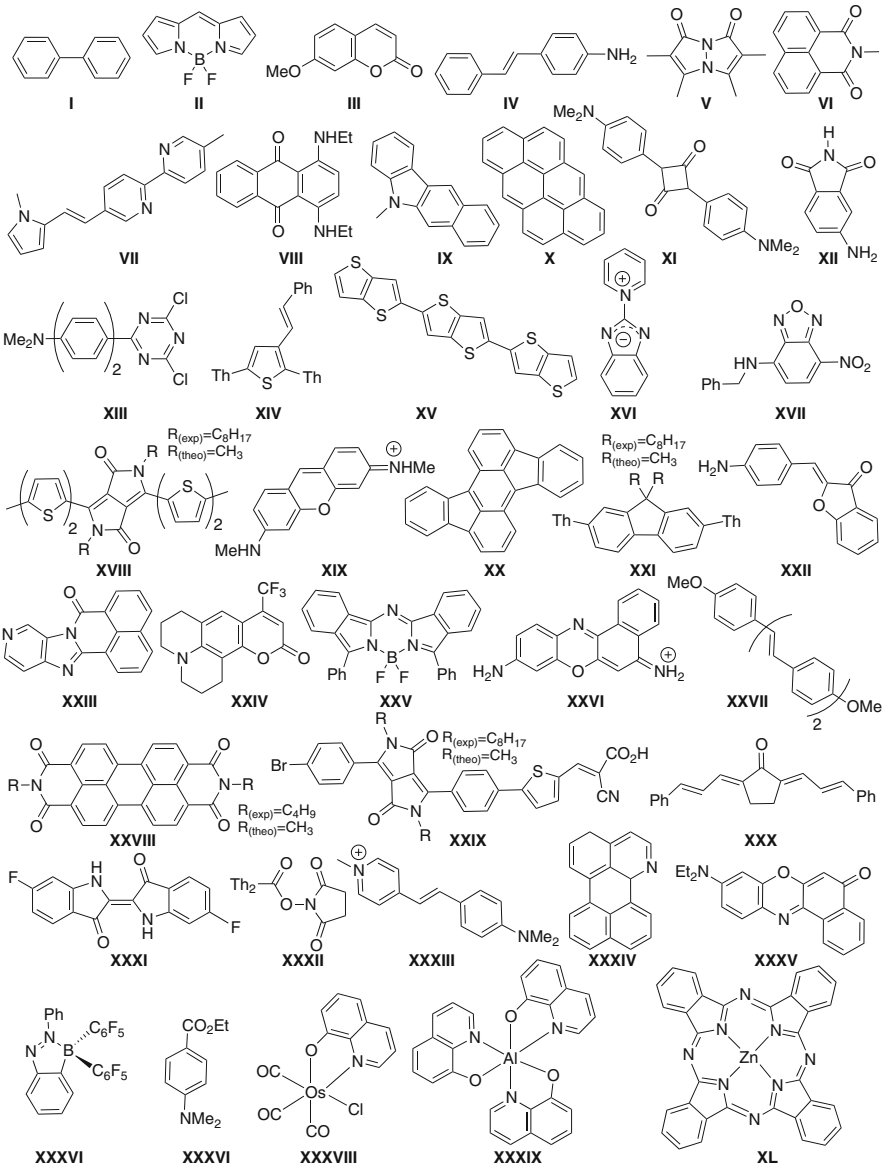

Fig. 2 Set of 40 test molecules used in several benchmarks of AFCP energies [15, 70, 71]. Reproduced with permissions from Jacquemin et al. [70]. Copyright 2014, American Chemical Society

and XCF dependence. For the 40 molecules displayed in Fig. 2, it has been found that the variations when changing the XCF are weak (ca. ± 0.02 eV) [15], a conclusion also reached in other studies on smaller systems [17, 66], indicating that ΔE^{ZPVE} can, in general, be evaluated with any XCF. In addition, this term was

Table 1 MSE and MAE obtained during benchmarks of E^{AFCP} of large structures. All data in eV. LC-PBE* and LC-PBE0* are optimally-tuned range-separated hybrid functionals

XCF	Molecular set	MSE	MAE	References
BP86	41 conjugated molecules	−0.56	0.57	[7]
BLYP	12 large dyes	−0.49	0.51	[13]
B3LYP	41 conjugated molecules	−0.33	0.34	[7]
	12 large dyes	−0.22	0.31	[13]
	40 dyes (Fig. 2)	−0.14	0.27	[15]
APF-D	40 dyes (Fig. 2)	−0.06	0.27	[71]
PBE0	40 dyes (Fig. 2)	−0.03	0.22	[15]
M06	40 dyes (Fig. 2)	0.05	0.23	[15]
PBE0-1/3	40 dyes (Fig. 2)	0.14	0.22	[71]
BMK	12 large dyes	0.07	0.19	[13]
SOGGA11-X	40 dyes (Fig. 2)	0.21	0.24	[70]
M06-2X	40 dyes (Fig. 2)	0.25	0.26	[15]
BHHLYP	41 conjugated molecules	−0.01	0.18	[7]
CAM-B3LYP	12 large dyes	0.11	0.18	[13]
	40 dyes (Fig. 2)	0.24	0.25	[15]
ωB97X-D	40 dyes (Fig. 2)	0.30	0.30	[70]
LC-PBE	40 dyes (Fig. 2)	0.56	0.57	[15]
LC-PBE*	40 dyes (Fig. 2)	0.12	0.20	[70]
LC-PBE0*	40 dyes (Fig. 2)	0.25	0.26	[71]
B2PLYP	12 large dyes	−0.11	0.20	[13]
B2GPPLYP	12 large dyes	−0.01	0.16	[13]

found to be non-negligible, e.g., it is −0.08 eV on average for the set of molecules shown in Fig. 2 [15]. Similar values have been obtained with other sets of molecules [13, 66].

With coworkers, we have investigated the E^{AFCP} of the compounds displayed in Fig. 2 using (10) and 12 XCF [15, 70, 71]. More precisely, we have used the LR-PCM model combined to the 6-31+G(d) atomic basis set for the geometrical and (harmonic) vibrational parameters whereas the electronic energies were computed at the cLR-PCM level with the 6-311++G(2df,2p) atomic basis set. The results of these works are summarized in Table 1 together with other works. In Table 1, the mean signed (MSE) and mean absolute (MAE) errors are given. Overall, one finds a general correlation between the amount of exact exchange included in the XCF and the MSE. Indeed, although PBE0 (25% exact exchange) [53, 62] is on average on the experimental spot (MSE close to 0), XCF including a larger fraction of exact exchange tend to yield positive MSE, i.e., they overestimate the experimental E^{AFCP}. This trend is quite general for low-lying ES: the larger the fraction of exact exchange included in the XCF, the larger the transition energies. However, the MAE tend to be quite similar for all approaches (ca. 0.25 eV), but for the LC-PBE range-separate hybrid [72] this is obviously not the most adequate approach in the present case. It should be noted that functionals such as M06-2X

[63, 64] and CAM-B3LYP [54] provide more consistent values, i.e., larger correlation coefficients with respect to experimental results (than B3LYP [52] or PBE0 [53, 62]) and can therefore be valued if design is sought: they overshoot the transition energies in a rather systematic way. The best results for the set of molecules of Fig. 2 are obtained with the optimally-tuned LC-PBE*, but at the cost of a systematic (non-empirical) optimization of the attenuation parameter.

Grimme and coworkers also performed a series of benchmarks [7, 13, 65] with a similar focus on "real-life" structures, and the results are collected in Table 1. In their first contribution, they evaluated 3 XCF (BP86 [59, 73], B3LYP [52], and BHLYP [74]) on 30 singlet–singlet and 13 doublet–doublet transitions in aromatic and radical dyes, respectively. Solvent effects were empirically accounted for by applying a standard correction to the experimental 0–0 energies. These authors concluded that global hybrids with 30–40% exact exchange emerged the best compromises [7]. More recently, the same group treated 12 molecules, transforming the measured energies in reference vertical values thanks to TD-DFT calculations. With this model, they could obtain deviations smaller than 0.2 eV with a recent global hybrid (BMK [75]), a range-separated hybrid (CAM-B3LYP [54]), and their double hybrid (B2GPPLYP [65]).

In short, the typical TD-DFT errors for E^{AFCP} are of the order of 0.2–0.3 eV, when hybrid XCF are used. It should also be noted that XCF including a large share of exact exchange (ca. 50%) deliver too large transition energies but tend to yield a good consistency (large correlation coefficient) with experiment. The most accurate results are obtained with double-hybrids or optimally-tuned range-separated XCF but for an increased computational effort.

3.2 Band Shapes

The accuracy of the band topologies obtained with several XCF has been evaluated by several groups [7, 16, 27, 71]. For the sake of consistency with the E^{AFCP} works presented above, we discuss here the two latter investigations which relied on a set of 20 conjugated molecules belonging to the same families as the one shown in Fig. 1. The selected protocol also relied on the 6-31+G(d) atomic basis set and included environmental effects thanks to the PCM approach. Selected key statistical data are given in Table 2. As all vibronic calculations have been performed on the basis of GS and ES vibrations obtained in the harmonic approximation, the clear trend is to overestimate the separation between the different vibronic peaks, irrespective of the selected XCF, an error which could be reduced by including anharmonic effects [16, 76, 77]. It is also obvious that the average absolute errors are smaller for absorption (ca. 100 cm^{-1}) than for emission (ca. 250 cm^{-1}). All XCF, apart from LC-PBE, provide rather similar deviations, and it is therefore difficult to select an unambiguously more accurate hybrid functional. Nevertheless, it should be noted that the obtained accuracy is significantly system dependent, e.g., most XCF are able to reproduce accurately the characteristic multi-peak structure of

Table 2 MSE and MAE obtained during benchmarks of the band shapes of absorption and emission spectra. The errors are given in cm^{-1} and correspond to difference of separation with the 0–0 peak which has been set to 0 cm^{-1} in both the theoretical and experimental spectra. All data have been taken in [16, 71]

	Absorption		Fluorescence	
XCF	MSE	MAE	MSE	MAE
B3LYP	51	80	80	225
APF-D	57	112	12	194
PBE0	63	117	115	263
M06	83	95	110	244
PBE0-1/3	89	134	47	227
SOGGA11-X	75	117	60	229
M06-2X	83	106	106	262
CAM-B3LYP	88	108	129	242
ωB97X-D	57	107	60	211
LC-PBE*	93	121	104	240
LC-PBE0*	120	139	87	235
LC-PBE	172	182	229	351

fused aromatics but they fail to provide the correct height of the shoulder in cyanines (see below for a discussion on the latter derivatives) [16]. For the relative intensities (setting the intensity of the most intense peak to 1), the typical TD-DFT error attains 10–15% for both absorption and emission, an average discrepancy which is again rather independent of the selected XCF. Eventually, as for E^{AFCP}, optimally-tuned approaches vastly improve the original LC-PBE results, though they do not outperform other XCF for band shapes. In other words, optimal tuning improves the transition energies without deteriorating the accuracy of the computed band shapes [71].

3.3 Challenging Cases

In this last part of this section, we consider a limited number of known TD-DFT problems for low-lying singlet ES. In these cases, the accuracy of TD-DFT is either worse than expected (cyanines) or can only be maintained with the selection of a specific XCF (charge-transfer). It should also be noted that triplet ES and, consequently, singlet-triplet splittings may be challenging for conventional TD-DFT [78–81] but this particular error is beyond our scope here.

3.3.1 Cyanine Excited-States

Cyanine derivatives are (positively or negatively) charged π-conjugated derivatives containing a linker possessing an odd number of sp^2 carbon atoms capped by two electronegative centers (typically, nitrogen, oxygen, or sulfur atoms). Both the canonical streptocyanines and the fluoroborate dyes (e.g., boron-dipyrromethene, BODIPY) belong to that class and it has been shown that they can hardly be

modeled with adiabatic TD-DFT [33, 82–93]. Indeed, the TD-DFT transition energies are too large (by ca. 0.3–1.0 eV) in cyanines, and this conclusion has been reached through comparisons of both TD-DFT's $E^{\text{vert}-\text{a}}$ with their highly-correlated wavefunction counterparts [82, 87] and TD-DFT's E^{AFCP} with experimental references for fluoroborate emitters [88, 89]. More puzzling is the fact that the errors seem to be almost independent of the selected XCF and that this error is not related to a multi-determinant nature. The fundamental reasons explaining this failure of TD-DFT have been given in [90–92, 94, 95] and summarized in a recent account [93]. A pragmatic approach to obtain accurate E^{AFCP} is to apply (13) selecting an appropriate variant of the CIS(D), ADC(2) or CC2 approaches as the wavefunction method [47, 96]. Examples of applications of such mixed approach are given in Sect. 4.

3.3.2 Energy and Geometry of Charge-Transfer States

One generally denotes as CT states, states in which the photon absorption or emission induces a strong displacement of the electronic density, i.e., when the electron and the hole are spatially separated. For those CT ES, it is now well recognized that both pure and global hybrid XCF including a small fraction of exact exchange tend to deliver (much) too small $E^{\text{vert}-\text{a}}$, $E^{\text{vert}-\text{f}}$, and E^{AFCP} [97–100]. For instance, Dreuw and Head-Gordon have shown that LDA [101], BLYP [59, 60], and B3LYP [52] XCF yield errors of 1 eV or more for the bacteriochlorophyll-spheroidene dyad. Within the adiabatic TD-DFT approximation, this error can be strongly reduced by using a range-separated hybrid XCF, e.g., CAM-3LYP [54], LC-BOP [102], or ωB97-X [103] which restores a correct interaction between the electron and the hole [104–107] and therefore provides an efficient answer to the CT challenge.

Additionally, the TD-DFT determination of the R^{ES} can be problematic for CT ES. Tozer was the first to unravel the qualitatively incorrect PES obtained for 4-(dimethylamino)-benzonitrile with B3LYP [108]. Indeed, this popular XCF predicts that the twisted ES, in which the NMe_2 terminal group becomes perpendicular to the central phenyl ring, is more stable than the corresponding planar geometry, whereas accurate wavefunction theories yield the opposite conclusion (more stable planar structure). As for the transition energies, the use of range-separated hybrid XCF restores a physically correct behavior. Similar conclusions to that of Tozer have been obtained for several other compounds [15, 109, 110] and it indicates that one should be particularly cautious when interpreting dual-fluorescence originating from an equilibrium between planar and twisted intramolecular CT.

In short, for CT states, both the structures and transition energies are more accurately evaluated using range-separated hybrid XCF.

4 Illustrations

4.1 Organic Electronic Chromophores

As stated previously, one of the advantages of computing vibrationally-resolved spectra is the access to both band topologies and absolute intensities, both data being unreachable with vertical calculations. We recently illustrated these aspects for a series of small organic chromophores used in organic electronics [111]. For three compounds proposed by Bäuerle and collaborators, a dramatic effect of the end groups was noted experimentally [112]. Indeed, adding terminal electro-accepting groups induces strong variations of the position, intensity, and shape of the optical curves. As illustrated in Fig. 3, the selected TD-DFT approach perfectly restores: (1) the auxochromic displacements related to substitution for both absorption and emission; (2) the relative intensities which are in a 1.0:1.9:3.4 ratio (see Fig. 3) for the black:blue:red spectra, matching the experimental values of 1.0:1.8:3.1; (3) the band shapes, especially the marked vibronic progression in the unsubstituted dye and the presence of strong shoulders for the substituted structures. In [111], 8 additional compounds have been studied for a total of 11 dyes, and the agreement between TD-DFT's band topologies and experimental data was found to be excellent in all cases but one. This is a remarkable result as the measured spectra often result from the overlapping contributions of several ES.

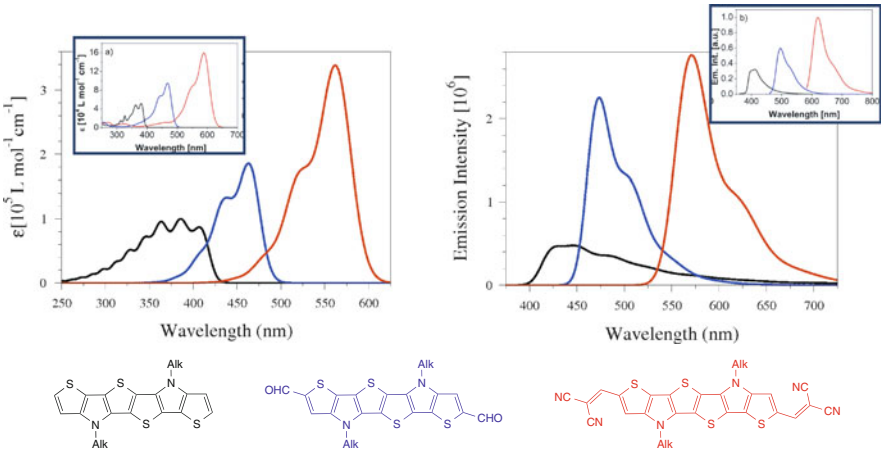

Fig. 3 Theoretical [cLR-PCM-M06/6-31+G(d)] absorption (*left*) and emission (*right*) band shapes obtained for three dyes (*bottom*). The experimental graphs are shown as *insets*. Adapted from [111] with permission from the Royal Society of Chemistry. No offset nor normalization was applied to the theoretical data. Experimental spectra adapted, with permission from Wetzel et al. [112]. Copyright 2014, American Chemical Society

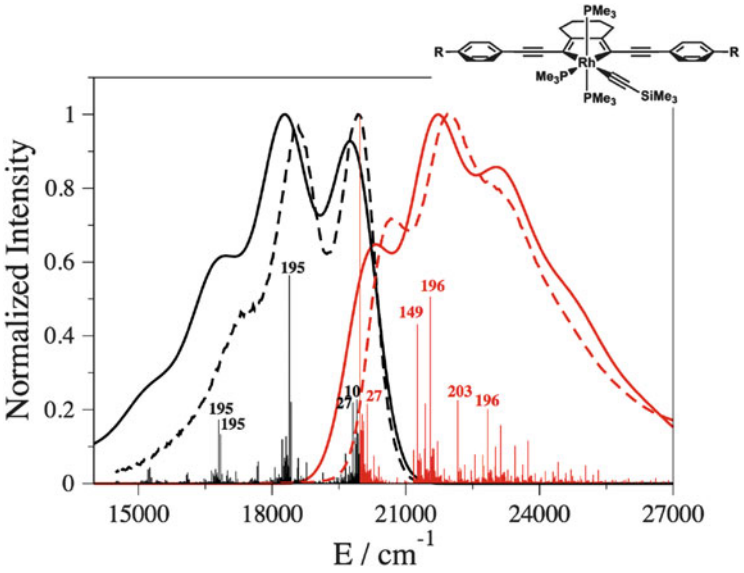

Fig. 4 Comparison between theoretical (*full lines*) and measured (*dashed lines*) absorption (*red*) and emission (*black*) band shapes of an inorganic complex. No shifting of the AFCP energies was applied. For the theoretical absorption and emission spectra, both the convoluted and stick spectra are displayed with numbering for the most contributing modes. Reproduced with permission from, Steffen et al. [115]. Copyright 2014, American Chemical Society

4.2 Inorganic Dyes

Although to date most applications of TD-DFT vibronic calculations have been performed for organic structures, there have also been several simulations for inorganic dyes [113–115]. An example of such successful work is given in Figure 4 that presents a direct comparison between measured and TD-DFT absorption and emission spectra for a rhodacyclopentadiene chromophore [115]. The good agreement is obvious: the AFCP energies are almost perfectly equal and the band topologies are also very close. Indeed, for emission, there are two peaks of nearly equivalent intensity followed by a shoulder whereas for the absorption, the 0–0 band is significantly less intense than the second peak. This good match confirmed that the complex experimental shapes originate from vibronic couplings and not from several energetically close electronic states. This finding was helpful to interpret several experimental outcomes [115]. For absorption (which is mostly influenced by ES vibrations), modes 27, 149, 196, and 203 appear at 160, 1290, 1578 and 2191 cm^{-1}, respectively. The second and third modes are mainly responsible for the most intense band at ca. 22000 cm^{-1}. These two vibrations correspond to stretchings of the double and single CC bonds of the rhodacycle.

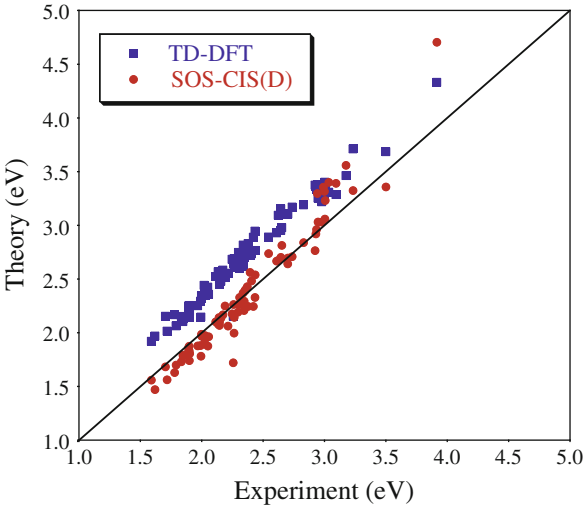

Fig. 5 Comparison between TD-DFT, SOS-CIS (D) and experimental 0–0 energies (eV) for a set of 83 fluoroborates. All TD-DFT calculations have been performed at the PCM-TD-M06-2X/6-311+G(2d,p)//PCM-M06-2X/6-31G(d) level, using either the cLR or the SS PCM approach for the transition energies. The *central line* indicates a perfect match between theory and experiment

4.3 Fluoroborate Derivatives

BODIPY and other similar derivatives relying on a fluoroborate group to ensure the chemical stability of the dyes constitute one of the most important classes of organic emitters [116–118]. Indeed, they present sharp fluorescence emission bands and large quantum yields. A large panel of chemical groups can be added around the central chromogens so as to modify the absorption and emission energies. These fluorophores present ES of cyanine nature, which is known to be challenging for TD-DFT (see above). Figure 5 displays the E^{AFCP} obtained with TD-DFT for a set of 83 fluoroborates using (10). This large set was obtained by putting together the panel of molecules considered in [47, 89, 96, 119] and was modeled using the M06-2X XCF. It is obvious that TD-DFT overestimates the E^{AFCP} in an almost systematic way (TD-DFT underestimates this energy in only 1 out of 83 cases), and this error is significant, as the MAE attains 0.354 eV. However, the variations of E^{AFCP} with the chemical structures is well reproduced by TD-DFT, and this can be seen by computing the linear determination coefficient, R^2, which attains 0.965 eV. This indicates that this protocol misses only 3.5% of the total variability of the experimental energies. To obtain values in better absolute agreement with experiment, it has been shown that applying a scaled opposite spin (SOS) variant of the CIS(D) model [45], that is using (13) with $\Psi = \mathrm{SOS\text{-}CIS(D)}$, is a very effective approach. Indeed, it allows the MAE to decrease by a factor of 3 (0.115 eV), at the same time inducing only a slight decrease of the R^2 (0.949). This is well illustrated in Fig. 5

Despite the systematic overestimation of the transition energy, it has been shown that TD-DFT allows reproduction of the band shapes of both the absorption and emission of fluoroborates with good to excellent accuracy [34, 35, 47, 88, 89, 120]. In other words, the PES provided by TD-DFT are reasonably accurate for

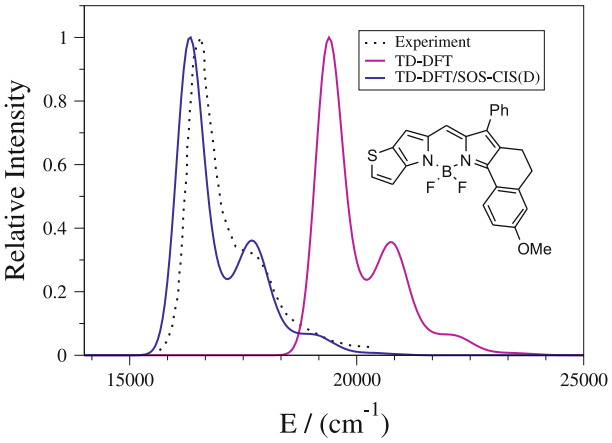

Fig. 6 Comparison between theoretical and experimental band topologies for a typical BODIPY derivative. The impact of the SOS-CIS(D) correction which shifts the E^{AFCP} is shown. Reproduced with permissions from Chibani et al. [47]. Copyright 2014, American Chemical Society

this class of dyes. This is illustrated in Fig. 6 for a strongly conjugated BODIPY designed to redshift the optical spectra. In Fig. 6 the band shape – which of course remains unchanged when applying the SOS-CIS(D) correction to the energy – clearly fits the experimental reference, with a marked shoulder displaced by ca. 1,500 cm^{-1} from the 0–0 band. The accuracy of TD-DFT's vibronic coupling has also been confirmed by computing the Huang–Rhys factors which were used to provide an estimation of the non-radiative deactivation vibrational pathways in selected BODIPY [89]. These factors correlated well with the measured quantum yields of emission: the larger the Huang–Rhys factors, the more efficient the non-radiative pathways, and the smaller the emission quantum yields.

4.4 ESIPT and Dual Emitters

Excited-state intramolecular proton transfer (ESIPT) is an extremely fast tautomerization process induced by photon absorption. ESIPT can take place in dyes presenting a strong intramolecular hydrogen bond, when the most stable isomer differs at the GS and ES. As illustrated in Fig. 7 for the typical enol/keto tautomerism, the structures of the absorbing and emitting species are strongly different, which advantageously yields very large Stokes shifts [121, 122]. Additionally, if the ES reaction is not quantitative, one can obtain emissions from both tautomers and hence reach dual fluorescence with a single compound [123]. This can be further optimized to design single-molecule white light emitting units [124], as ESIPT quantum yield tends to increase when going from solution to solid state.

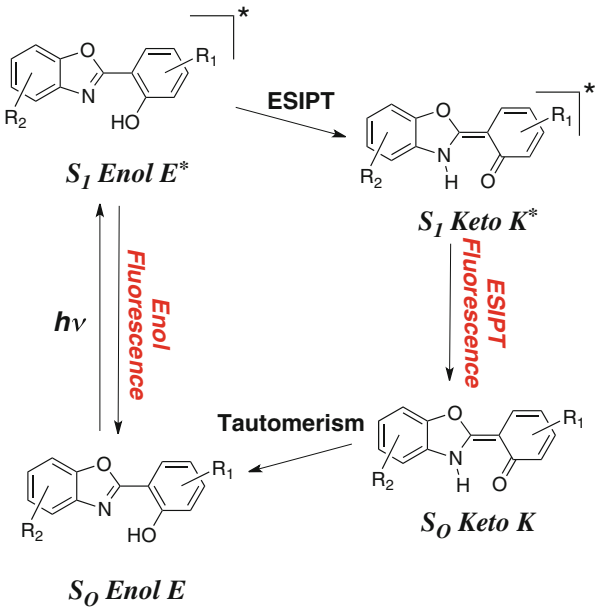

Fig. 7 Schematic representation of an ESIPT system containing an enol and a keto isomer. Adapted with permissions from Benelhadj et al. [124]. Copyright 2014, Wiley

There are numerous applications of TD-DFT and wavefunction approaches to rationalizing excited-state proton transfer [124–144] and, for the sake of consistency, we summarize here some of the works that have been performed with an approach similar to that used in the previous section, i.e., cLR-PCM/TD-M06-2X [124, 139–141]. Houari et al. explored the GS and ES PES of two hydroxyphenylbenzoxazole (HBO) dyes, differing only by their end groups [123, 139]. The alkyl-substituted system only shows emission from the keto tautomer experimentally, whereas the amino-substituted compound displays (dual-)emission from both enol and keto tautomers [123]. Houari et al. obtained the PES of both the GS and the ES (see Fig. 8) which helped to rationalize the experimental trends. Indeed, for the dye presenting sole ESIPT emission, the PES of the ES presents only a small transition state which disappears when vibrational corrections are included. In other words, after photon absorption there is a downhill slope for the ESIPT reaction on the free energy scale and only the keto isomer corresponds to a true minimum and can emit light. For the second dye (right panel in Fig. 8), the transition state is higher in energy and the enol minimum on the ES surface applies once vibrational corrections are included, indicating that dual emission is feasible. These conclusions fit the corresponding experimental data perfectly [123]. Figure 8 also shows that the transition states for the proton transfer are located at very different geometries for the GS and the ES, e.g., at respective O–H distances of 1.410 and 1.185 Å, for the first dye, indicating that a simple vertical TD-DFT calculation performed on the GS transition state would fail to deliver valuable insights. In the same work [139], the computed vibrationally-resolved emission spectra were compared to experiment to allow an approximate determination of the relative quantum yields of enol and keto

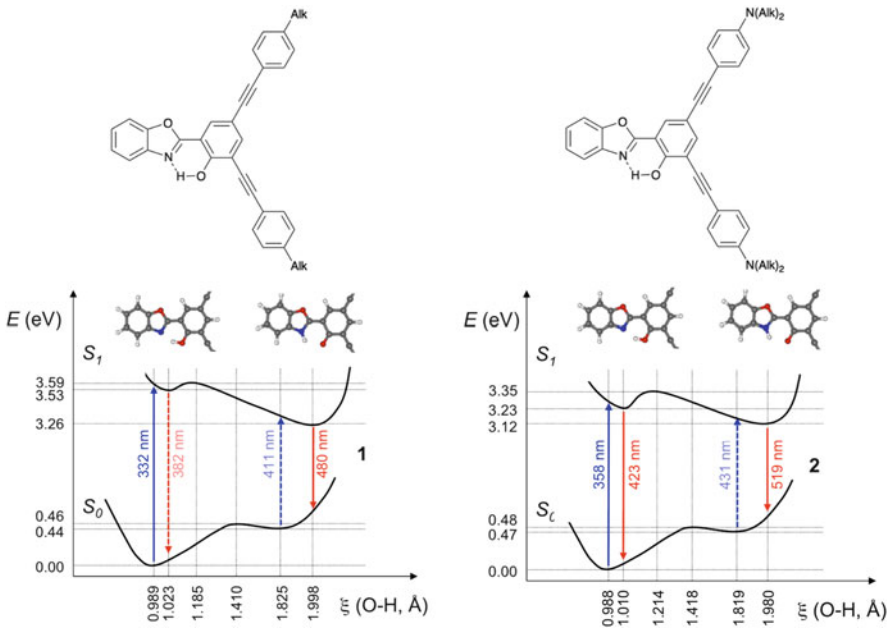

Fig. 8 Potential energy surfaces obtained for two HBO dyes. *Left*: alkyl substituted structure presenting only ESIPT emission experimentally. *Right*: amino-substituted structure displaying dual fluorescence in several solvents. For both dyes, the PES go from the enol (small O–H distance) to the keto (large O–H distance). Adapted from Houari et al. [139] with permission from the Royal Society of Chemistry

emission for a solvent in which the measured fluorescence bands for these two tautomers overlap.

In a subsequent investigation [124], TD-DFT was used to rationalize the properties of seven large hydroxybenzofuranbenzoxazole (HBBO) derivatives differing by their substitution patterns. A comparison between the experimental ratio of ESIPT and normal emissions (I^{keto}/I^{enol}) with the theoretical relative stabilities of the two tautomers determined for the ES (ΔG^{ES}) is given in Fig. 9. When the ΔG^{ES} are smaller than −0.1 eV, the driving force is sufficient to yield a quantitative proton transfer and only ESIPT emission is observed. Between −0.1 and 0.0 eV, there is an equilibrium between the two forms which emit and dual emission can only be obtained in this narrow energetic window. The correlation between the measured relative fluorescence intensities and the computed driving force for ESIPT is obvious in Fig. 9. This study led to the development of single-molecule white organic light emitting diodes [124].

4.5 Caging Effects

As stated above, TD-DFT can be coupled with several models to reproduce the impact of the environment on the spectral properties of a chromophore. Besides the

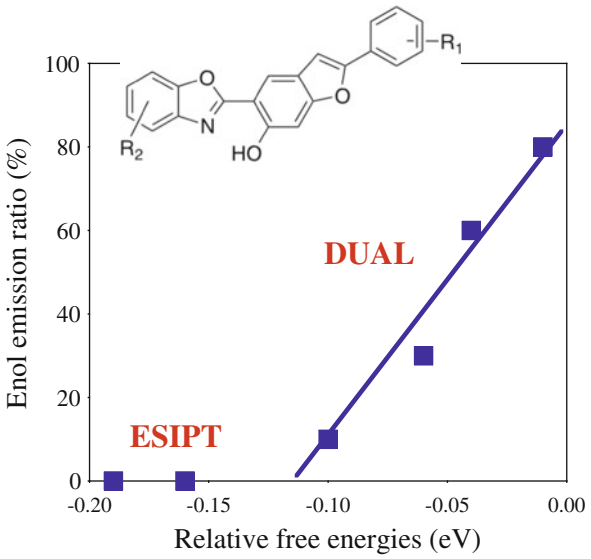

Fig. 9 Comparison between the theoretical relative free energies of the enol and keto isomers determined at the ES and the experimentally observed ratio of enol emission. See Benelhadj et al. [124]

most widely treated case of organic solvents, such an environment can involve a biomolecule [145–148], a cage [149, 150] a metal [151–153], an inorganic solid [154–156], or a molecular crystal [157] to cite a few examples. Depending on the exact nature of the environment, one needs to set up a specific computational protocol, but the general idea is to split the total system into two parts: the chromophore where the electronic excitation takes place and which is treated with TD-DFT whereas the surroundings are modeled with a simpler theoretical model, typically Molecular Mechanics (MM). We illustrate here such a procedure for an organic cage and redirect interested readers to a previous review on the topic for other examples and references [27]. The selected system consists of a squaraine dye encapsulated in a tetralactam macrocycle (see Fig. 10). Such an assembly was experimentally investigated by Smith and coworkers [158] and later modeled [149]. The macrocyclic cage aims to protect the dye from (bio-)chemical degradations and was not designed to tune the observed color. Indeed, the hallmark absorption band of the dye is shifted after complexation by −0.06 eV only [158], a bathochromic effect which can be almost perfectly reproduced by TD-DFT calculations considering the full system quantum mechanically (−0.07 eV). However, such a brute force approach implies a large computational cost. As the excitation is clearly localized on the squaraine, using a hybrid TD-DFT/MM is justified. The first approach proposed in [149] was to account self-consistently for the ground-state polarization by determining atomic point charges of the cage equilibrated with the density of the dye. Such a procedure yields a qualitatively incorrect hypsochromic shift of +0.10 eV. In a second approach, the response of the cage density to the change of electronic state of the dye was modeled through a

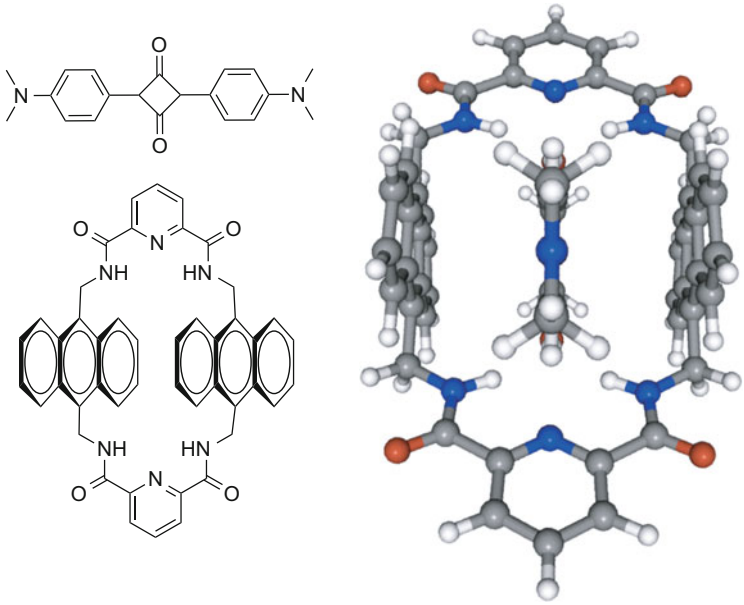

Fig. 10 Representation of the squaraine dye (*top left*) and cage (*bottom left*) used by Smith and coworkers [158]. On the right hand side, a side view of the DFT (PBE0) optimized complex is given [149]

polarizable continuum model inspired from PCM. This second scheme, denoted Electronic Response of the Surroundings, yields, for a negligible computational cost, a shift of −0.09 eV, in good agreement with both experiment and full TD-DFT calculation.

4.6 Charge-Transfer Optimization

Photoinduced charge-transfer excited states play a key role in several applications, notably in dye sensitized solar cells (DSSC) [159–163]. In DSSC, the absorption of light by a dye anchored on a semi-conducting surface, typically a metallic oxide, induces a CT on the dye which eventually leads to charge separation, the electron (or the hole) being injected into the semi-conductor. Charge transfer is therefore the key step initiating the light-to-electricity conversion process [164]. To quantify CT, several schemes have been proposed [56, 165–168] and we present here the d^{CT} index [165, 166]. This approach uses the ground- and excited-states electronic densities (ρ^{GS} and ρ^{ES}) to provide a CT distance (d^{CT}), the amount of charge transferred (q^{CT}), and CT dipole (μ^{CT}). First one computes the difference of densities between the excited and ground states:

$$\Delta\rho(\mathbf{r}) = \rho^{\mathrm{ES}}(\mathbf{r}) - \rho^{\mathrm{GS}}(\mathbf{r}). \tag{14}$$

Subsequently, one divides $\Delta\rho(\mathbf{r})$ into two parts according to the increase/decrease of the density resulting from the electronic transition. For the former, this reads

$$\rho^{+}(\mathbf{r}) = \begin{cases} \Delta\rho(\mathbf{r}) & \text{if} \quad \Delta\rho(\mathbf{r}) > 0 \\ 0 & \text{if} \quad \Delta\rho(\mathbf{r}) < 0\,, \end{cases} \tag{15}$$

and similarly for $\rho^{-}(\mathbf{r})$. The amount of charge transferred is obtained by integration

$$q^{\mathrm{CT}} = \int \rho^{+}(\mathbf{r}) d\mathbf{r}, \tag{16}$$

and an equivalent result is obtained by integrating $\rho^{-}(\mathbf{r})$. One next computes the barycenters corresponding to the $\rho^{+}(\mathbf{r})$ and $\rho^{-}(\mathbf{r})$ functions

$$r^{+} = (x^{+}, y^{+}, z^{+}) = \frac{1}{q^{\mathrm{CT}}} \int \mathbf{r}\rho^{+}(\mathbf{r}) d\mathbf{r}, \tag{17}$$

$$r^{-} = (x^{-}, y^{-}, z^{-}) = \frac{1}{q^{\mathrm{CT}}} \int \mathbf{r}\rho^{-}(\mathbf{r}) d\mathbf{r}. \tag{18}$$

The distance separating these two points is the CT distance

$$d^{\mathrm{CT}} = \sqrt{(x^{+} - x^{-})^2 + (y^{+} - y^{-})^2 + (z^{+} - z^{-})^2}, \tag{19}$$

whereas the CT dipole is

$$\left|\left|\mu^{\mathrm{CT}}\right|\right| = d^{\mathrm{CT}} q^{\mathrm{CT}}. \tag{20}$$

μ^{CT} is also equal to the difference of dipoles computed from the total GS and ES densities. This procedure was applied to design rod-like dyes with a maximal CT distance, using densities obtained with TD-DFT and more precisely with the CAM-B3LYP functional [169]. The compounds considered in [169] consist of an electron-donor group and an electron-acceptor moiety separated by a π-conjugated linker. All parameters were investigated (nature of the donor, size and nature of the linker, strength of the acceptor. . .). An illustration of the results obtained is given in Fig. 11 for three typical push–pull systems. For the shortest system, one indeed notices a typical CT state, the nitro (amino) group gaining (losing) density upon electronic excitation and d^{CT} is large. When the π-conjugated chain gets longer, one observes, contrary to expectations, that d^{CT} decreases. This can be qualitatively understood from Fig. 11: as the chain gets longer the excited-state starts to be

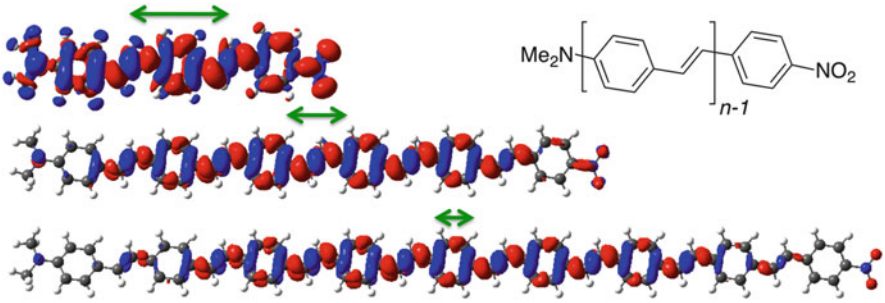

Fig. 11 Representation of $\Delta\rho(\mathbf{r})$ for three oligomers (trimer, hexamer, and nonamer). The *green vector* indicates the CT distance. The *blue* (*red*) regions indicate decrease (increase) of density after photon absorption. Adapted with permission from Ciofini et al. [169]. Copyright 2012, American Chemical Society

localized on the central part of the dye, with a minimal involvement of the terminal groups and the CT character is lost, because the excited-state eventually corresponds to a delocalized but symmetric $\pi \rightarrow \pi^\star$ transition. This means that, to maximize CT, there is an optimal linker length. For α,ω-NMe_2,NO_2 oligomers, this maximal CT is obtained for an oligomeric length of ca. 3–5 connecting rings, smaller (larger) systems being limited by the lack of efficient delocalization (the ineffective communication between the end groups). In [169] it was therefore concluded that *there is a systematic fine balance between the three elements of the rod-like compounds, and simply increasing the strength of the terminal electro-active groups or improving the delocalizability by adding more π-electrons in the bridge does not necessarily mean improvement of the CT properties.*

5 Conclusions

Theoretical spectroscopy in general, and Time-Dependent Density Functional Theory in particular, have now become mature tools to reproduce, predict, and interpret both absorption and emission spectra of a wide range of "real-life" molecules in "real-life" environments. TD-DFT is regularly applied as a black-box model to complement experimental measurements. As illustrated in this review, TD-DFT is now used not only to probe the nature of excited states within the vertical approximation, but also to determine 0–0 energies and band shapes for compounds containing up to ca. 150 atoms. These more demanding, but more insightful, simulations will undoubtedly become increasingly popular in the near future. Another key advantage of TD-DFT is that it can be coupled to several models for describing several kinds of environmental effects (solvents, cages, metals, surfaces…). Although some wavefunction approaches can be more accurate for specific systems, their less favorable scaling with system size remains an important limitation to their applicability to extended systems. The main weakness

of the adiabatic approximation to TD-DFT is its exacerbated dependency on the selected XCF. Nevertheless, the know-how is actually so great in this field that one can often easily select an adequate functional for the molecule and state considered. In the following years, it should become a common approach to combine TD-DFT geometries and vibrational frequencies to wavefunction vertical excitation energies so as to improve the accuracy of the final results and decrease the functional dependency. At the same time, the focus moves from the "static" spectral properties to "dynamic" excited-state reactions (proton-transfer, energy transfer photochromism. . .).

Acknowledgements D.J. acknowledges the European Research Council (ERC) and the *Région des Pays de la Loire* for financial support in the framework of a Starting Grant (Marches – 278845) and a *recrutement sur poste stratégique*, respectively. The COST-CMTS Action CM1002: COnvergent Distributed Environment for Computational Spectroscopy (CODECS) and its members are acknowledged for many fruitful discussions.

References

1. Runge E, Gross EKU (1984) Phys Rev Lett 52:997
2. Casida ME (1995) Time-dependent density-functional response theory for molecules. In: Recent advances in density functional methods, vol 1. World Scientific, Singapore, pp 155–192
3. Dreuw A, Head-Gordon M (2005) Chem Rev 105:4009
4. Ullrich C (2012) Time-dependent density-functional theory: concepts and applications. Oxford Graduate Texts (Oxford University Press), New York
5. Casida ME, Huix-Rotllant M (2012) Annu Rev Phys Chem 63:287
6. Laurent AD, Adamo C, Jacquemin D (2014) Phys Chem Chem Phys 16(28):14334
7. Dierksen M, Grimme S (2004) J Phys Chem A 108:10225
8. Fortrie R, Chermette H (2007) J Chem Theory Comput 3:852
9. Santoro F, Lami A, Improta R, Bloino J, Barone V (2008) J Chem Phys 128:224311
10. Guthmuller J, Zutterman F, Champagne B (2008) J Chem Theory Comput 4(2):2094
11. Peltier C, Laine PP, Scalmani G, Frisch MJ, Adamo C, Ciofini I (2009) J Mol Struct (THEOCHEM) 914:94
12. Improta R, Santoro F, Barone V, Lami A (2009) J Phys Chem A 113(52):15346
13. Goerigk L, Grimme S (2010) J Chem Phys 132:184103
14. Lopez GV, Chang CH, Johnson PM, Hall GE, Sears TJ, Markiewicz B, Milan M, Teslja A (2012) J Phys Chem A 116(25):6750
15. Jacquemin D, Planchat A, Adamo C, Mennucci B (2012) J Chem Theory Comput 8:2359
16. Charaf-Eddin A, Planchat A, Mennucci B, Adamo C, Jacquemin D (2013) J Chem Theory Comput 9:2749
17. Winter NOC, Graf NK, Leutwyler S, Hattig C (2013) Phys Chem Chem Phys 15:6623
18. van Caillie C, Amos RD (1999) Chem Phys Lett 308:249
19. Furche F, Ahlrichs R (2002) J Chem Phys 117:7433
20. Scalmani G, Frisch MJ, Mennucci B, Tomasi J, Cammi R, Barone V (2006) J Chem Phys 124:094107
21. Liu F, Gan Z, Shao Y, Hsu CP, Dreuw A, Head-Gordon M, Miller BT, Brooks BR, Yu JG, Furlani TR, Kong J (2010) Mol Phys 108(19–20):2791
22. Liu J, Liang WZ (2011) J Chem Phys 135(18):184111

23. Barbatti M, Crespo-Otero R (2015) Density-functional methods for excited states. In: Ferré N, Filatov M, Huix-Rotllant M (eds) Topics in current chemistry. Springer, Berlin/Heidelberg, pp 1–30. doi:10.1007/128_2014_605
24. Laurent AD, Jacquemin D (2013) Int J Quantum Chem 113:2019
25. Ziegler T, Krykunov M, Cullen J (2012) J Chem Phys 136:124107
26. Tomasi J, Mennucci B, Cammi R (2005) Chem Rev 105:2999
27. Jacquemin D, Mennucci B, Adamo C (2011) Phys Chem Chem Phys 13:16987
28. Cammi R, Mennucci B (1999) J Chem Phys 110:9877
29. Cossi M, Barone V (2001) J Chem Phys 115:4708
30. Caricato M, Mennucci B, Tomasi J, Ingrosso F, Cammi R, Corni S, Scalmani G (2006) J Chem Phys 124:124520
31. Improta R, Scalmani G, Frisch MJ, Barone V (2007) J Chem Phys 127:074504
32. Marenich AV, Cramer CJ, Truhlar DG, Guido CG, Mennucci B, Scalmani G, Frisch MJ (2011) Chem Sci 2:2143
33. Jacquemin D, Zhao Y, Valero R, Adamo C, Ciofini I, Truhlar DG (2012) J Chem Theory Comput 8:1255
34. Chibani S, Charaf-Eddin A, Le Guennic B, Jacquemin D (2013) J Chem Theory Comput 9:3127
35. Chibani S, Charaf-Eddin A, Mennucci B, Le Guennic B, Jacquemin D (2014) J Chem Theory Comput 10(2):805
36. Andersson K, Malmqvist P, Roos BO (1992) J Chem Phys 96(2):1218 http://scitation.aip.org/content/aip/journal/jcp/96/2/10.1063/1.462209
37. Buenker RJ, Peyerimhoff SD (1968) Theor Chim Acta 12(3):183
38. Stanton JF, Bartlett RJ (1993) J Chem Phys 98(9):7029
39. Christiansen O, Koch H, Jørgensen P (1995) Chem Phys Lett 243:409
40. Kállay M, Gauss J (2004) J Chem Phys 121(19):9257
41. Hättig C, Weigend F (2000) J Chem Phys 113:5154
42. Nakatsuji H, Ehara M (1993) J Chem Phys 98:7179
43. Schirmer J, Trofimov AB (2004) J Chem Phys 120:11449
44. Head-Gordon M, Maurice D, Oumi M (1995) Chem Phys Lett 246:114
45. Rhee YM, Head-Gordon M (2007) J Phys Chem A 111(24):5314
46. Boulanger P, Chibani S, Le Guennic B, Duchemin I, Blase X, Jacquemin D (2014) J Chem Theory Comput 10(10):4548
47. Chibani S, Laurent AD, Le Guennic B, Jacquemin D (2014) J Chem Theory Comput 10:4574
48. Guthmuller J, Zutterman F, Champagne B (2009) J Chem Phys 131:154302
49. Improta R, Barone V (2009) J Mol Struct (THEOCHEM) 914(1–3):87
50. Avila Ferrer FJ, Improta R, Santoro F, Barone V (2011) Phys Chem Chem Phys 13(38):17007
51. Avila Ferrer FJ, Santoro F (2012) Phys Chem Chem Phys 14(39):13549
52. Becke AD (1993) J Chem Phys 98:5648
53. Adamo C, Barone V (1999) J Chem Phys 110:6158
54. Yanai T, Tew DP, Handy NC (2004) Chem Phys Lett 393:51
55. Chai JD, Head-Gordon M (2008) Phys Chem Chem Phys 10:6615
56. Peach MJG, Benfield P, Helgaker T, Tozer DJ (2008) J Chem Phys 128:044118
57. Picconi D, Avila Ferrer FJ, Improta R, Lami A, Santoro F (2013) Faraday Discuss 163:223
58. Ciofini I, Adamo C (2007) J Phys Chem A 111:5549
59. Becke AD (1988) Phys Rev A 38:3098
60. Lee C, Yang W, Parr RG (1988) Phys Rev B 37:785
61. Perdew JP, Burke K, Ernzerhof M (1996) Phys Rev Lett 77:3865
62. Ernzerhof M, Scuseria GE (1999) J Chem Phys 110:5029
63. Zhao Y, Truhlar DG (2008) Acc Chem Res 41:157
64. Zhao Y, Truhlar DG (2008) Theor Chem Accounts 120:215
65. Goerigk L, Moellmann J, Grimme S (2009) Phys Chem Chem Phys 11:4611
66. Send R, Kühn M, Furche F (2011) J Chem Theory Comput 7(8):2376

67. Bates JEE, Furche F (2012) J Chem Phys 137:164105
68. Barnes L, Abdul-Al S, Allouche AR (2014) J Phys Chem A 118(46):11033, PMID: 25350349
69. Fang C, Oruganti B, Durbeej B (2014) J Phys Chem A 118:4157
70. Jacquemin D, Moore B, Planchat A, Adamo C, Autschbach J (2014) J Chem Theory Comput 10(4):1677
71. Moore B, Charaf-Eddin A, Planchat A, Adamo C, Autschbach J, Jacquemin D (2014) J Chem Theory Comput 10(10):4599
72. Song JW, Hirosawa T, Tsuneda T, Hirao K (2007) J Chem Phys 126:154105
73. Perdew JP (1986) Phys Rev B 33:8822
74. Becke AD (1993) J Chem Phys 98:1372
75. Boese AD, Martin JML (2004) J Chem Phys 121:3405
76. Biczysko M, Bloino J, Brancato G, Cacelli I, Cappelli C, Ferretti A, Lami A, Monti S, Pedone A, Prampolini G, Puzzarini C, Santoro F, Trani F, Villani G (2012) Theor Chem Accounts 131(4):1201
77. Stendardo E, Ferrer FA, Santoro F, Improta R (2012) J Chem Theory Comput 8(11):4483
78. Jacquemin D, Perpète EA, Ciofini I, Adamo C (2010) J Chem Theory Comput 6:1532
79. Peach MJG, Williamson MJ, Tozer DJ (2011) J Chem Theory Comput 7(11):3578
80. Sears JS, Koerzdoerfer T, Zhang CR, Brédas JL (2011) J Chem Phys 135:151103
81. Peach MJG, Tozer DJ (2012) J Phys Chem A 116(39):9783
82. Fabian J (2001) Theor Chem Accounts 106:199
83. Schreiber M, Bub V, Fülscher MP (2001) Phys Chem Chem Phys 3:3906
84. Grimme S, Neese F (2007) J Chem Phys 127:154116
85. Jacquemin D, Perpète EA, Scalmani G, Frisch MJ, Kobayashi R, Adamo C (2007) J Chem Phys 126:144105
86. Fabian J (2010) Dyes Pigm 84:36
87. Send R, Valsson O, Filippi C (2011) J Chem Theory Comput 7(2):444
88. Chibani S, Le Guennic B, Charaf-Eddin A, Maury O, Andraud C, Jacquemin D (2012) J Chem Theory Comput 8:3303
89. Chibani S, Le Guennic B, Charaf-Eddin A, Laurent AD, Jacquemin D (2013) Chem Sci 4:1950
90. Moore B II, Autschbach J (2013) J Chem Theory Comput 9:4991
91. Filatov M, Huix-Rotllant M (2014) J Chem Phys 141(2):024112
92. Zhekova H, Krykunov M, Autschbach J, Ziegler T (2014) J Chem Theory Comput 10:3299
93. Le Guennic B, Jacquemin D (2015) Acc Chem Res 48:530
94. Ziegler T, Krykunov M, Seidu I, Park Y (2015) Density-functional methods for excited states. In: Ferré N, Filatov M, Huix-Rotllant M (eds) Topics in current chemistry. Springer, Berlin/Heidelberg, pp 1–35. doi:10.1007/128_2014_611
95. Filatov M (2015) Density-functional methods for excited states. In: Ferré N, Filatov M, Huix-Rotllant M (eds) Topics in current chemistry. Springer, Berlin/Heidelberg. doi:10.1007/128_2014_630
96. Charaf-Eddin A, Le Guennic B, Jacquemin D (2014) RSC Adv 4:49449
97. Tozer DJ, Amos RD, Handy NC, Roos BO, Serrano-Andrès L (1999) Mol Phys 97:859
98. Cai ZL, Sendt K, Remiers R (2002) J Chem Phys 117:5543
99. Gritsenko OV, Baerends EJ (2004) J Chem Phys 121:655
100. Dreuw A, Head-Gordon M (2004) J Am Chem Soc 126:4007
101. Vosko SJ, Wilk L, Nusair M (1980) Can J Phys 58:1200
102. Iikura H, Tsuneda T, Yanai T, Hirao K (2001) J Chem Phys 115:3540
103. Chai JD, Head-Gordon M (2008) J Chem Phys 128:084106
104. Tawada T, Tsuneda T, Yanagisawa S, Yanai T, Hirao K (2004) J Chem Phys 120:8425
105. Rudberg E, Salek P, Helgaker T, Agren H (2005) J Chem Phys 123:184108
106. Cai ZL, Crossley MJ, Reimers JR, Kobayashi R, Amos RD (2006) J Phys Chem B 110:15624
107. Lange AW, Rohrdanz MA, Herbert JM (2008) J Phys Chem B 112:6304
108. Wiggins P, Gareth Williams JA, Tozer DJ (2009) J Chem Phys 131:091101

109. Plötner J, Tozer DJ, Dreuw A (2010) J Chem Theory Comput 6(8):2315
110. Guido CA, Mennucci B, Jacquemin D, Adamo C (2010) Phys Chem Chem Phys 12:8016
111. Charaf-Eddin A, Cauchy T, Felpin FX, Jacquemin D (2014) RSC Adv 4:55466
112. Wetzel C, Mishra A, Mena-Osteritz E, Liess A, Stolte M, Würthner F, Bäuerle P (2014) Org Lett 16(2):362. doi:10.1021/ol403153z. http://pubs.acs.org/doi/abs/10.1021/ol403153z
113. Lanthier E, Reber C, Carrington T Jr (2006) Chem Phys 329(1–3):90, Electron correlation and multimode dynamics in molecules (in honour of Lorenz S. Cederbaum)
114. Latouche C, Baiardi A, Barone V (2015) J Phys Chem B (in press)
115. Steffen A, Costuas K, Boucekkine A, Thibault MH, Beeby A, Batsanov AS, Charaf-Eddin A, Jacquemin D, Halet JF, Marder TB (2014) Inorg Chem 53(13):7055
116. Loudet A, Burgess K (2007) Chem Rev 107:4891
117. Ulrich G, Ziessel R, Harriman A (2008) Angew Chem Int Ed 47:1184
118. Nepomnyashchii AB, Bard AJ (2012) Acc Chem Res 45(11):1844
119. Chibani S, Laurent AD, Le Guennic B, Jacquemin D (2015) J Phys Chem A. PMID:25522826
120. Zakrzewska A, Zalesny R, Kolehmainen E, Osmialowski B, Jedrzejewska B, Agren H, Pietrzak M (2013) Dyes Pigm 99(3):957
121. Henary MM, Wu Y, Fahrni CJ (2004) Chem Eur J 10(12):3015
122. Wu Y, Peng X, Fan J, Gao S, Tian M, Zhao J, Sun S (2007) J Org Chem 72(1):62
123. Massue J, Ulrich G, Ziessel R (2013) Eur J Org Chem 2013(25):5701
124. Benelhadj K, Muzuzu W, Massue J, Retailleau P, Charaf-Eddin A, Laurent AD, Jacquemin D, Ulrich G, Ziessel R (2014) Chem Eur J 20:12843
125. Sobolewski AL, Domcke W (1999) Phys Chem Chem Phys 1:3065
126. Aquino AJA, Lischka H, Hattig C (2005) J Phys Chem A 109:3201
127. Aquino AJA, Plasser F, Barbatti M, Lischka H (2009) Croat Chem Acta 82:105
128. Barbatti M, Aquino AJA, Lischka H, Schriever C, Lochbrunner S, Riedle E (2009) Phys Chem Chem Phys 11:1406
129. Plasser F, Barbatti M, Aquino AJA, Lischka H (2009) J Phys Chem A 113(30):8490
130. Randino C, Ziolek M, Gelabert R, Organero JA, Gil M, Moreno M, Lluch JM, Douhal A (2011) Phys Chem Chem Phys 13:14960
131. Cui G, Lan Z, Thiel W (2012) J Am Chem Soc 134(3):1662
132. Xie L, Chen Y, Wu W, Guo H, Zhao J, Yu X (2012) Dyes Pigm 92(3):1361
133. Hayaki S, Kimura Y, Sato H (2013) J Phys Chem B 117(22):6759
134. Moreno M, Ortiz-Sanchez JM, Gelabert R, Lluch JM (2013) Phys Chem Chem Phys 15:20236
135. Padalkar VS, Ramasami P, Sekar N (2013) J Fluoresc 23(5):839
136. Phatangare KR, Gupta VD, Tathe AB, Padalkar VS, Patil VS, Ramasami P, Sekar N (2013) Tetrahedron 69(6):1767
137. Savarese M, Netti PA, Adamo C, Rega N, Ciofini I (2013) J Phys Chem B 117(50):16165
138. Savarese M, Netti PA, Rega N, Adamo C, Ciofini I (2014) Phys Chem Chem Phys 16:8661
139. Houari Y, Charaf-Eddin A, Laurent AD, Massue J, Ziessel R, Ulrich G, Jacquemin D (2014) Phys Chem Chem Phys 16:1319
140. Laurent AD, Houari Y, Carvalho PHPR, Neto BAD, Jacquemin D (2014) RSC Adv 4:14189
141. Hubin PO, Laurent AD, Vercauteren DP, Jacquemin D (2014) Phys Chem Chem Phys 16:25288
142. Wilbraham L, Savarese M, Rega N, Adamo C, Ciofini I (2015) J Phys Chem B 119:2459
143. Raucci U, Savarese M, Adamo C, Ciofini I, Rega N (2015) J Phys Chem B 119:2650
144. Houari Y, Chibani S, Jacquemin D, Laurent AD (2015) J Phys Chem B 119:2180
145. Riccardi D, Schaefer P, Yang Y, Yu H, Ghosh N, Prat-Resina X, Konig P, Li G, Xu D, Guo H, Elstner M, Cui Q (2006) J Phys Chem B 110(13):6458
146. Wanko M, Hoffmann M, Frähmcke J, Frauenheim T, Elstner M (2008) J Phys Chem B 112 (37):11468
147. Konig C, Neugebauer J (2011) Phys Chem Chem Phys 13:10475

148. Curutchet C, Kongsted J, Munoz-Losa A, Hossein-Nejad H, Scholes GD, Mennucci B (2011) J Am Chem Soc 133:3078
149. Jacquemin D, Perpète EA, Laurent AD, Assfeld X, Adamo C (2009) Phys Chem Chem Phys 11:1258
150. Garcia G, Ciofini I, Fernández-Gómez M, Adamo C (2013) J Phys Chem Lett 4(8):1239
151. Masiello DJ, Schatz GC (2010) J Chem Phys 132:064102
152. Morton SM, Jensen L (2010) J Chem Phys 133:074103
153. Sanchez-Gonzalez A, Corni S, Mennucci B (2011) J Phys Chem C 115(13):5450
154. Onida G, Reining L, Rubio A (2002) Rev Mod Phys 74:601
155. Tilocca A, Fois E (2009) J Phys Chem C 113(20):8683
156. Labat F, Le Bahers T, Ciofini I, Adamo C (2012) Acc Chem Res 45(8):1268
157. Presti D, Labat F, Pedone A, Frisch MJ, Hratchian HP, Ciofini I, Menziani MC, Adamo C (2014) J Chem Theory Comput 10:5577
158. Gassensmith JJ, Arunkumar E, Barr L, Baumes JM, DiVittorio KM, Johnson JR, Noll BC, Smith BD (2007) J Am Chem Soc 129:15054
159. Odobel F, Le Pleux L, Pellegrin Y, Blart E (2010) Acc Chem Res 43:1063
160. Lin HC, Jin BY (2010) Materials 3(8):4214
161. Planells M, Pelleja L, Clifford JN, Pastore M, De Angelis F, Lopez N, Marder SR, Palomares E (2011) Energy Environ Sci 4:1820
162. Zhao Y, Liang W (2012) Chem Soc Rev 41:1075
163. Le Bahers T, Pauporté T, Lainé PP, Labat F, Adamo C, Ciofini I (2013) J Phys Chem Lett 4 (6):1044
164. Kalyanasundaram K, Grätzel M (1998) Coord Chem Rev 177:347
165. Le Bahers T, Adamo C, Ciofini I (2011) J Chem Theory Comput 8:2498. Code available at Chimie Paristech, www.chimie-paristech.fr/labos/LECA/Research/site_msc/
166. Jacquemin D, Le Bahers T, Adamo C, Ciofini I (2012) Phys Chem Chem Phys 14:5383. Code available at Université de Nantes, http://www.sciences.univ-nantes.fr/CEISAM/erc/marches/ . Accessed 1 May 2014
167. Guido CA, Cortona P, Mennucci B, Adamo C (2013) J Chem Theory Comput 9(7):3118
168. Etienne T, Assfeld X, Monari A (2014) J Chem Theory Comput 10(9):3906
169. Ciofini I, Le Bahers T, Adamo C, Odobel F, Jacquemin D (2012) J Phys Chem C 116:11946, erratum: *ibidem* 14736–14736